ISSN 1547-4771, Physics of Particles and Nuclei Letters, 2023, Vol. 20, No. 4, pp. 872–879. © Pleiades Publishing, Ltd., 2023.
Russian Text © The Author(s), 2023, published in Pis'ma v Zhurnal Fizika Elementarnykh Chastits i Atomnogo Yadra, 2023.

PHYSICS AND TECHNIQUE OF ACCELERATORS

Testing of Magnetic Elements of the Electron Cooling System for the NICA Collider

V. B. Reva[a, b, *], A. M. Batrakov[a], M. I. Bryzgunov[a], A. V. Bubley[a], R. V. Vakhrushev[a], K. M. Gorchakov[a, b], V. K. Gosteev[a], A. P. Denisov[a], M. N. Kondaurov[a], V. M. Konstantinov[a], V. Ya. Korchagin[a], N. S. Kremnev[a], V. M. Panasyuk[a], V. V. Parkhomchuk[a], S. P. Pospolita[a], A. A. Putmakov[a], and K. S. Shtro[a, b]

[a] *Budker Institute of Nuclear Physics, Siberian Branch, Russian Academy of Sciences, Novosibirsk, 630090 Russia*
[b] *Novosibirsk State University, Novosibirsk, 630090 Russia*
**e-mail: V.B.Reva@inp.nsk.su*

Received November 18, 2022; revised December 16, 2022; accepted January 23, 2023

Abstract—In order to achieve the design luminosity in the NICA collider, the rings are planned to be equipped with stochastic and electron cooling. The 2.5 MeV electron cooling system consists of two coolers that cool both ion beams simultaneously. This report deals with the design of the electron cooler and the results of testing of its magnetic elements at the Budker Institute of Nuclear Physics, Siberian Branch, Russian Academy of Sciences (BINP SB RAS).

DOI: 10.1134/S1547477123040568

INTRODUCTION

To date, QCD has been well studied at high energies. However, experimental data in the low and medium energy region, which are important for understanding the internal structure and dynamics of hadrons, are insufficient; therefore, the precision spectroscopy of these energy ranges is an urgent task. The desire to be able to experiment with high-quality beams with average energy gave impetus to the development of NICA (Russia), FAIR (Germany), and HIAF (China). The implementation of physical experiments in the energy range up to 4.5 GeV/n requires the use of various types of cooling (electronic and stochastic) in order to improve the quality of charged particle beams. To do this, the NICA complex will be equipped with two cooling systems: stochastic and electron. The electron cooling system (ECS) should provide an electron beam with an electron energy of up to 2.5 MeV and a direct current of up to 1 A.

1. ECS DESIGN

The electron cooling system for the NICA collider consists of two practically independent electron cooling systems (Fig. 1). The closest analogue of the NICA ECS in terms of design and underlying physical principles is the electron cooling for the COSY storage ring for energies up to 2 MeV [1]. The entire high-voltage system of each NICA cooler is located in a separate tank with SF_6 gas under pressure up to 8 atm. The electron beam is generated in the gun located in the tank and accelerated in the electrostatic tube to the required energy. The beam enters the cooling section through the transport channel, where it interacts with ions. Then, through another transport channel, the beam returns to the tank, where it slows down in the second electrostatic tube and is absorbed on the walls of the electron collector. All the way from the gun to the collector, the electrons move in a longitudinal magnetic field to provide transverse focusing. In medium and low-energy electron cooling systems a strong longitudinal magnetic field is used, the electron trajectories are tied to the force lines, and one can speak that motion is "magnetized," when a large value of the transverse momentum of particles has little effect on their trajectories. With an increase in the electron energy, the situation changes significantly, so any inhomogeneity of the longitudinal magnetic field introduces a perturbation of the electron beam trajectory, leading to the excitation of the Larmor rotation, which can reduce the cooling rate. Despite the availability of special correctors to compensate for it, the need to obtain the primary optics of the electron beam leading to the minimum Larmor rotation remains critical.

For the most efficient use of the place allocated for the NICA collider ECS, the cooling sections of both coolers are located one above the other and have the same length. Electron beams in them, like ion beams, will move in opposite directions.

Figure 2 shows examples of the implementation of the main magnetic elements for transporting an elec-

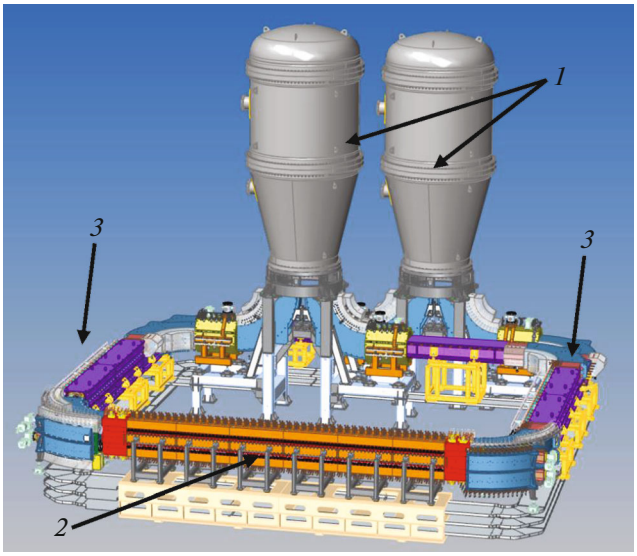

Fig. 1. Three-dimensional model of the ECS of the NICA collider: (*1*) high-voltage system tank, (*2*) cooling section, (*3*) transport channels.

tron beam. Particularly difficult conditions are imposed on the region where the ion and proton beams coincide. Here it is necessary to provide such a profile of the change in the longitudinal magnetic field with ~2 kG in the cooling section (Fig. 2 on the left, *1*) up to ~1 kG in the toroidal section (Fig. 2 on the left, *3*), which would minimally perturb the transverse motion of electrons. For this, a matching section is used (Fig. 2 on the left, *2*), where the longitudinal position of the coils is selected based on the results of magnetic modeling. The coils of the toroidal section are of different sizes to ensure the alignment of the ion and electron beam transport channels.

The transition between the straight section of the transport channel (Fig. 2 on the left, *5*) and the toroidal section was also made using a specialized insert section (Fig. 2 on the left, *4*). Despite the fact that here the value of the longitudinal magnetic field is the same, the coils of the insert section have a minimum length. Then, due to their shift in the longitudinal direction, it is possible to provide a place for the technological assembly of the vacuum chamber, placement of pickup wire leads, and short corrector coils to reduce the cyclotron rotation of the electron beam. The value of the longitudinal field was chosen to implement magnetized cooling and electron beam optics. At the same time, a reasonable compromise is required between energy consumption and the achievable value of the magnetic field; therefore, the value of the magnetic field in the transport channels is reduced compared to the cooling section in order to achieve an energy consumption of the system of 500–700 kW [2].

2. MAGNETIC MEASUREMENT SYSTEM

To compare the results of calculations of magnetic fields using the specialized MAG3D program and the results of measurements, a set of elementary guides was used consisting of straight segments of various lengths and a turn of 90° with a radius of 100 cm. With their help, it is possible to measure almost any set of magnetic elements (see Fig. 3). In this case, it is preferable to measure as part of a triad, when two adjacent elements are attached to the main element for a more correct measurement of the edge effects of the magnetic field. Figure 4 shows a photograph of a system of magnetic elements for measuring a bending magnet.

To move the magnetic field sensor, a flexible toothed one-sided Elatech polyurethane belt (type M

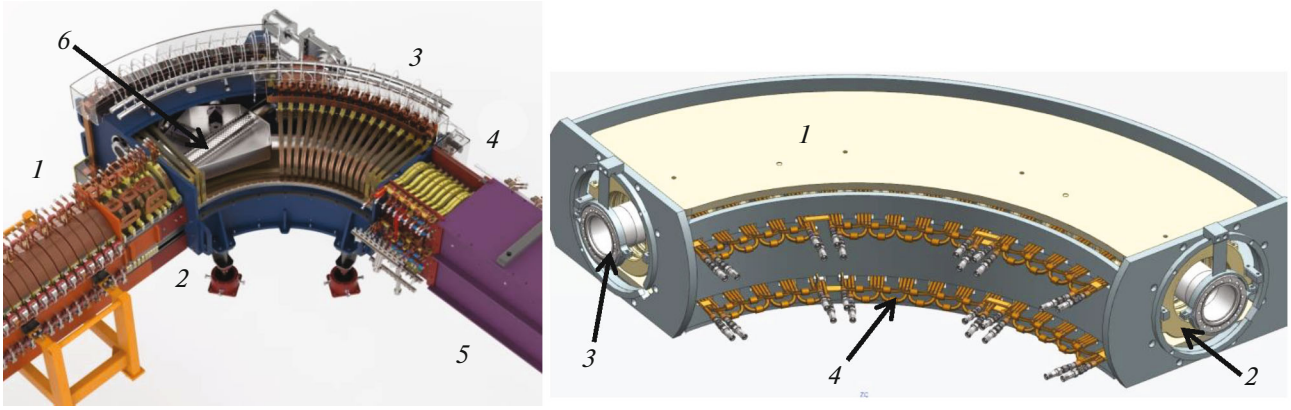

Fig. 2. Three-dimensional model of the ion and proton beam superposition area in the ECS of the NICA collider (left): (*1*) cooling section, (*2*) matching section, (*3*) toroidal section, (*4*) insert section, (*5*) straight section of the transport channel, and (*6*) vacuum chamber. 3D model of a swing magnet (right): (*1*) bending (vertical) field coil, (*2*) longitudinal field coil, (*3*) vacuum chamber, and (*4*) terminals of longitudinal field coils.

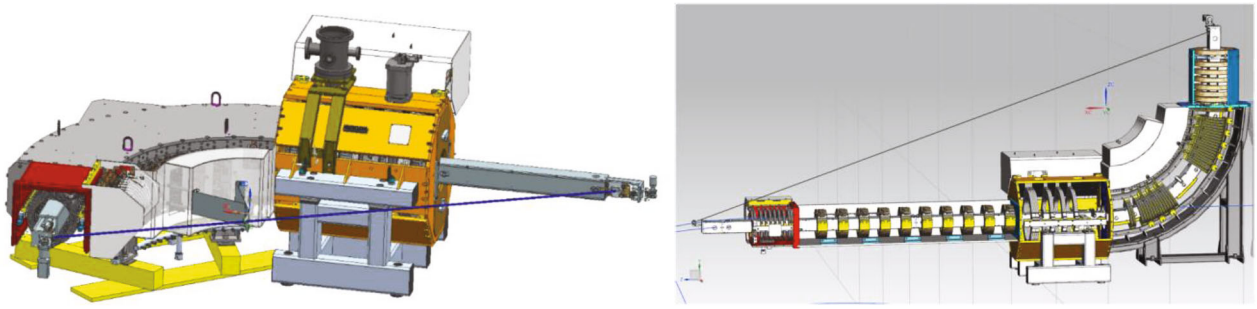

Fig. 3. 3D model of a magnetic measurement system in a bending magnet in combination with adjacent elements (left) and the maximum possible set of magnetic elements for measurement as part of a single design (right).

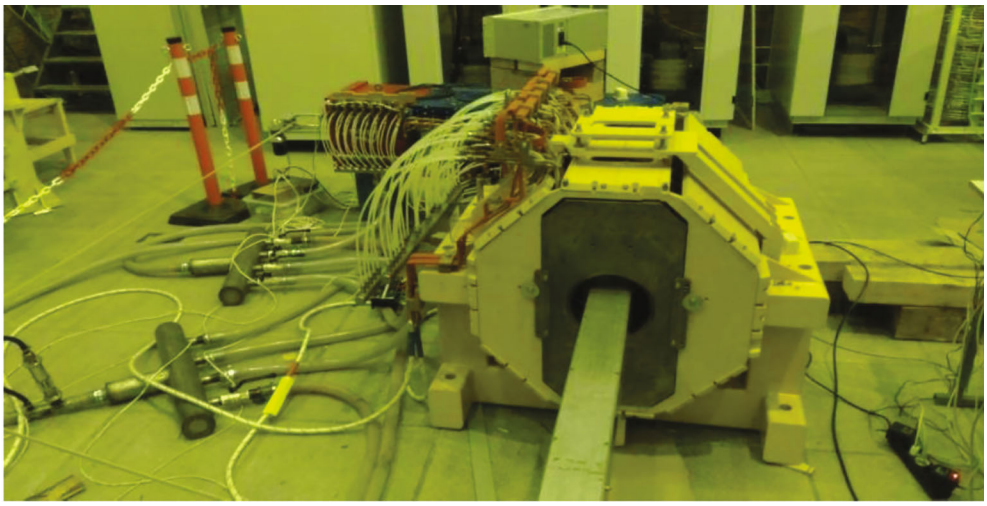

Fig. 4. System of magnetic measurements in a bending magnet.

(open) with an aramid cord) was used: profile T5 (pitch 5 mm) and width of 10 mm.

The magnetic field sensor holder was mounted on a movable carriage that could move along the magnetic elements. The position of the carriage along the rails was used as the longitudinal coordinate.

2.1. Three-Axis Magnetic Field Sensor

Electron cooling systems have high requirements for the transverse components of the solenoidal magnetic field. For the high-quality cooling of ion beams, it is necessary to have transverse components in the cooling section (B_x, B_y) at level 10^{-5} relative to the longitudinal component of the magnetic field B_z [3, 4]. Since the longitudinal field of the cooling section has the value ~2 kG; then the order of magnitude of the transverse components to be measured is from 0.01 to 0.1 G. To determine the components of such a small value, the Budker Institute of Nuclear Physics, Siberian Branch, Russian Academy of Sciences (BINP SB RAS), developed the Compass system [4]. This system uses a 4-quadrant photodiode to measure the deflection of a laser beam reflected from a mirror sensitive to transverse field components. However, such supersensitive systems are of little use for magnetic fields on the order of 10 gauss. Therefore, to measure the parameters of the transverse components of the magnetic fields in the cooling section and in the transport channels, "rough" measurements with Hall sensors in the range of 0.1–10 G are also required.

To this end, the BINP has been using for many years a system consisting of the following electronic modules installed in the VME crate: BIVME-1 controller, VME RS-232 interface, VMEHSI analog Hall sensor interface with a 32-channel multiplexer and amplifier, and a precision ADC VMEADC [5]. To move the carriage with a step of 0.5–10 mm along the magnetic device, a stepper motor is used, controlled via the RS-232 interface. The coordinate of the carriage in the magnetic device is determined by the number of steps taken. After the end of the measurement, the carriage with the sensor in continuous mode returns back 10 mm further than the starting position,

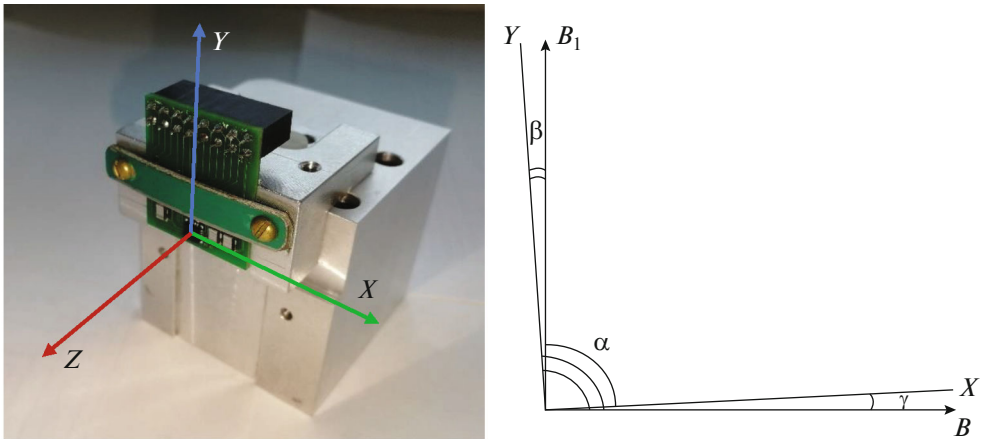

Fig. 5. Calibration cube with "sensor + board + carrier" kit installed without a communication cable between the board and the measuring electronics. On the right is a diagram for determining the angles characterizing the nonorthogonality of the Hall sensors.

after which it moves forward by the same 10 mm, compensating for the mechanical hysteresis of the movement. As a result, it is possible to achieve a repeatability of passages at the level of ±50–80 μm. The amplified Hall sensor signals from the analog interface are transmitted to a 24-bit ADC capable of measuring with a resolution of 0.1 gauss (determined mainly by the system's own noise) and an accuracy no worse than 2×10^{-5} from the full measuring range (which is determined by the temperature stability of the electronics).

The Metrolab MV2 chip was used as a 3D (three-coordinate) Hall sensor. The sensor itself is made using integrated technology and, in addition to the Hall converter, also contains a stabilized power supply and a programmable amplifier that allows it to operate in several ranges of magnetic fields. The nominal sensitivity of the sensor in the range of interest to us (±3 kG) is 0.7 mV/G for the Z axis and 0.65 mV/G for the X and Y axes with a linearity of 0.2% of the scale and a stability of about 250 ppm/K [6]. However, it should be noted that the manufacturer of the 3D sensor does not specify the orthogonality of its magnetic axes.

The measurement of sensitivity and nonorthogonality was carried out using a "calibration cube" made of nonmagnetic aluminum alloy with three orthogonal faces with a deviation of no more than 10 μm on a base of 50 mm. On one of the faces of the cube, a board carrier was mounted in the form of a corner, on which a board with a 3D sensor was installed (Fig. 5). Subsequently, the corner with the board was fixed in the carriage. Installing the carrier on the calibration cube made it possible to measure the complete nonorthogonality of the "sensor + board + carrier" combination, abandoning intermediate separate measurements.

During calibration, this assembly was placed in a dipole magnet with a uniform magnetic field, the value of which was determined using a precision NMR magnetometer with a measurement error of about 2 ppm [7]. The calibration assembly was installed on one of the planes of the cube at the pole of the magnet, the field in which is perpendicular to the pole and, accordingly, to the plane of the calibration cube. To determine the sensitivity and nonorthogonality, the field was measured at 18 points in the range of ±3 kG. Next, the cube was alternately placed on two other planes, and the procedure was repeated.

Determining the intrinsic nonorthogonality of the axes of the three-dimensional sensor MV2 can be reduced either to solving three two-dimensional problems (Fig. 5) or to constructing a transformation matrix that diagonalizes the experimentally measured values to orthogonal axes chosen as a basis. For the XY plane, the angles were $\beta = 0.008$ rad, $\gamma = 0.006$ rad. When measuring the fields of cooling solenoids and transport channels of the NICA ECS, a large longitudinal field component can have a great influence B_z to small values of the transverse components of the magnetic field (B_x and B_y); therefore, to analyze the results, it is necessary to know the angle γ for the coordinate systems ZX (0.025 rad.) and ZY (0.007 rad.).

2.2. Results of Measurements of the Longitudinal Field with a Three-Component Sensor

The results of measurements of the longitudinal field for several bending magnets are shown in Figs. 6, 7. In our measurements, the X direction of the sensor was oriented along the vertical direction of the rotary magnet and Y was oriented along the radial direction. The longitudinal direction corresponded to the Z axis of the three-component sensor. It can be seen that, for a longitudinal field of 1 kG (see Fig. 6), the vertical component in the magnet is $B_v = 20$ G and radial is $B_r = 40$ G (see Fig. 7). The radial component can be explained by the displacement of the center of the magnetic field sensor relative to the wheels of the

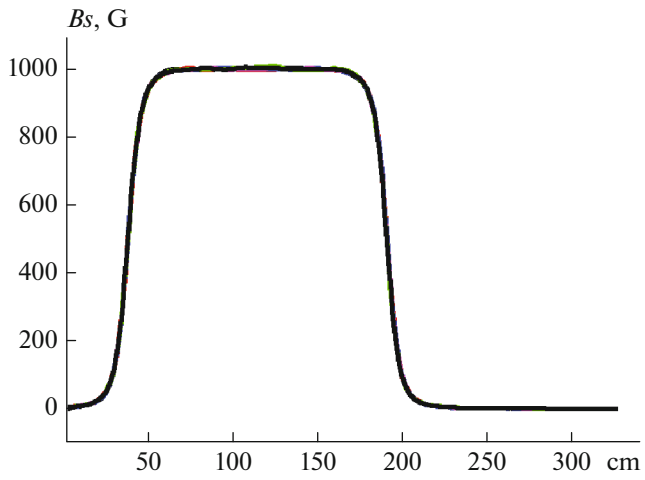

Fig. 6. Longitudinal magnetic field in a bending magnet at current J_{sbend} = 195 A.

carriage, which ensure the movement of the sensor along the guides (Fig. 8). The field sensor goes almost above the frontmost wheels of the cart, so it describes the trajectory with good accuracy: line–arc–line, but at the same time on the arc it turns out to be inclined in the radial-longitudinal plane by an angle of 0.04 rad. The vertical component of the magnetic field appears due to the nonorthogonality of the corresponding Hall sensors (see Section 2.1).

After eliminating the above connection between the magnetic field components, it became possible to compare the magnetic field components with the simulation results. Figure 9 shows the experimental and calculated value of the radial and vertical magnetic fields, as well as the difference between the experiment and calculations for the longitudinal component. A fairly good agreement between them is seen. At the same time, in this design, the geometry of the magnetic circuit is not a determining factor for the formation of a magnetic field. Uncertainties associated with the switching wire leads and the position of the copper conductors relative to the measuring planes and the outer frame of the coils of the longitudinal field are possible.

2.3. Spatial Sensor Based on 12 Hall Sensors

The measurements described in point 2.2 allow measuring the distribution of the magnetic field only along the center line of the bending magnet. For magnetic measurements in a certain area near it, a calibrated set of 12 Hall sensors was used. They were placed on a special cross-shaped holder in such a way that three components of the magnetic field were measured and each component was measured at four points around the center line of the solenoid. Figure 10 shows the design of the cross holder together with the carriage. The distance between points 1–2 and 3–4 is 30 mm. The offset of the Hall sensors within one spatial point is 5 mm. Using a linear approximation, all values were recalculated to a transverse position of 15 mm relative to the center of the cruciform holder and to one longitudinal position. To reduce the influence of the angles between the sensors arising from inaccuracies in the manufacture of faces and errors when gluing the Hall sensors to them, a calibration procedure was carried out in a magnet according to the same procedure as for a 3-component sensor. Thus, a matrix of transformations of the measured values of the magnetic field to three fixed orthogonal projections was obtained.

2.4. Results of Measurements of the Bending Field near the Axis of the Bending Magnet

The results of measurements at a current in the coil of the bending field J_{bend} = 270 A are shown in Figs. 11 and 12. It can be seen that the measured values are in good agreement with the simulation results and look

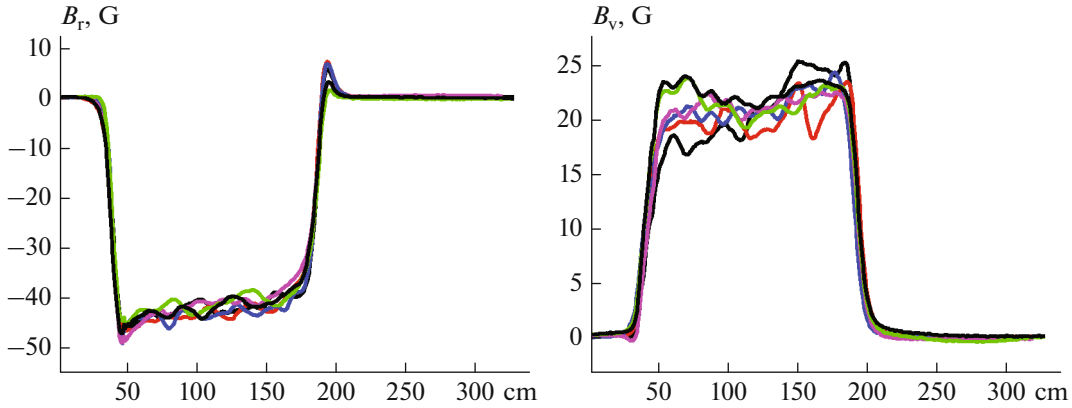

Fig. 7. Transverse components of the magnetic field in a bending magnet at current J_{sbend} = 195 A. The current in the vertical field coil is zero.

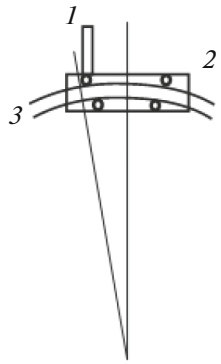

Fig. 8. Sketch explaining the appearance of an angle between the longitudinal and radial components of the magnetic field caused by the noncentral location of the Hall sensor. (*1*) Magnetic field sensor together with the board, (*2*) carriage for moving the sensor, and (*3*) curved guide.

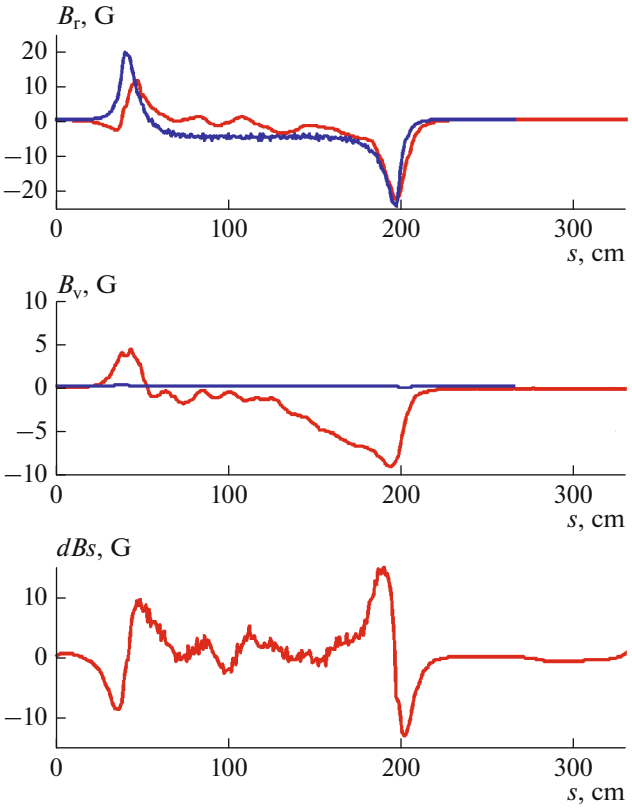

Fig. 9. Comparison of experimental (red curve) and calculated data (blue curve) when a longitudinal magnetic field of 1 kG is turned on in bending magnets.

even more symmetrical and plausible in detail in the edge regions. The latter is due to the complexity of modeling complex coils in the selected software package. At the edge of the magnet, one can clearly see the longitudinal magnetic field that arises above and below the plane of rotation due to the fulfillment of

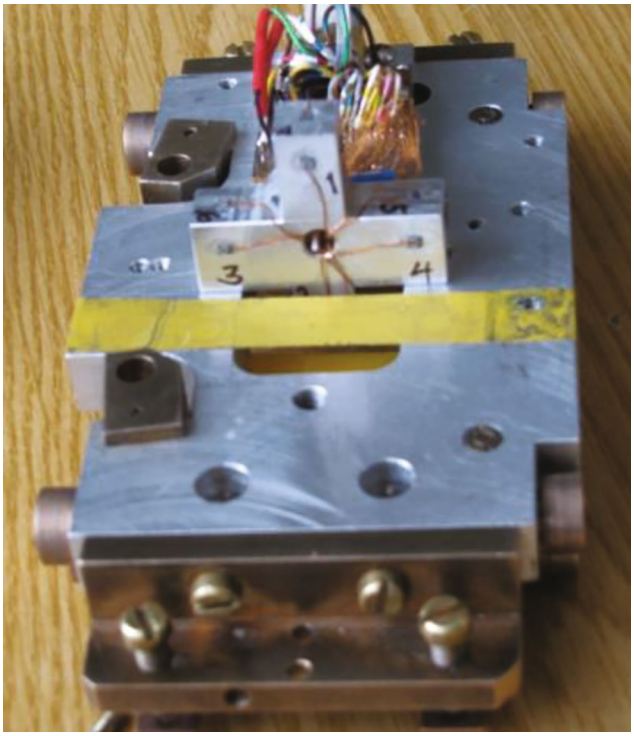

Fig. 10. Cross-shaped holder for Hall sensors together with carriage. The numbers indicate the points of the cross at which the magnetic field components are measured.

Maxwell's equations (see Fig. 12). The symmetry of these values allows us to judge how accurately we pass through the magnetic center of our turn, as well as how accurately it coincides with the center of the structure of our turn obtained during the mechanical exhibition of the measurement system. This must be controlled, since the position of the magnetic circuit is weakly related to the configuration of the magnetic field, and everything is determined by the accuracy of the location of the coils of the rotary and leading fields.

Spatial measurements of the vertical magnetic field also make it possible to estimate its field index n, which can be defined as

$$b_1 = \frac{1}{2}\left(\frac{dB_r}{dv} + \frac{dB_v}{dr}\right), \quad n = -R\frac{b_1}{B_v},$$

where B_r and B_v are the radial and vertical components of the magnetic field, R is the bending radius, and v is the vertical coordinate. Here we have used the equality

$$\mathrm{rot}(\vec{B}) = 0 \;\Rightarrow\; \frac{dB_r}{dv} = \frac{dB_v}{dr}$$

to increase the experimental accuracy of determining this parameter.

Figure 13 shows that, over the entire length of the magnet, coefficient $b_1 = 0.5$ g/cm, and $n = 0.45$, which is close to the expected value $n = 0.5$ when designing this element. The choice of this value is due to the

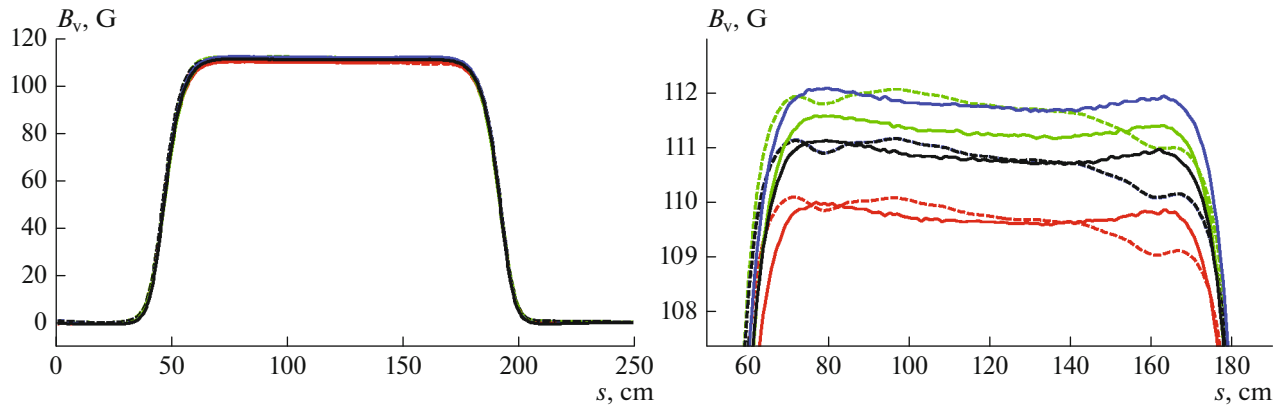

Fig. 11. Vertical magnetic field in a 90° bending magnet. On the left, a more detailed distribution is shown in the region where it reaches a constant value. The solid curves are the experimentally measured values; the dotted lines are the simulation results.

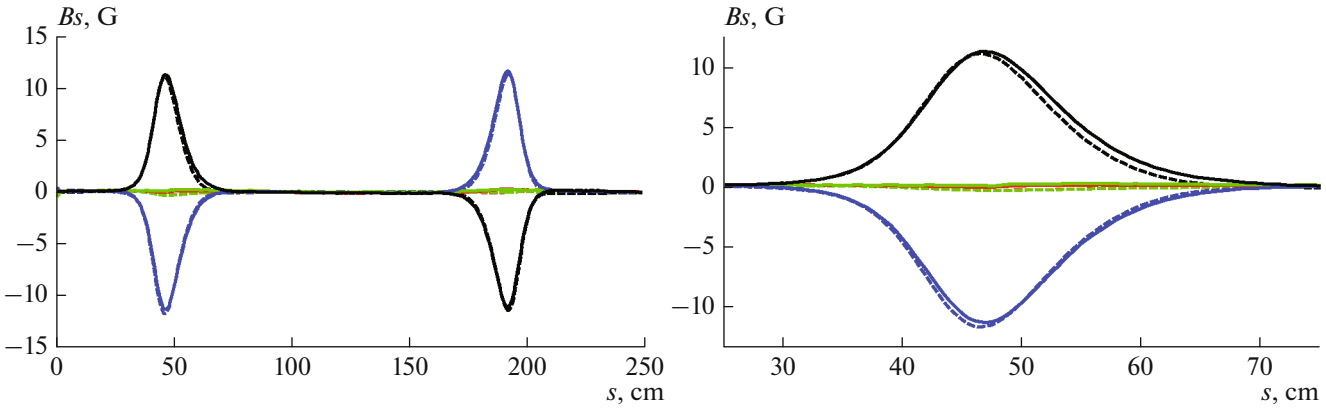

Fig. 12. Longitudinal magnetic field in a 90° bending magnet when the bending field is turned on. On the left, its more detailed distribution is shown when entering (exiting) a bend. The solid curves are the experimentally measured values; the dotted lines are the simulation results.

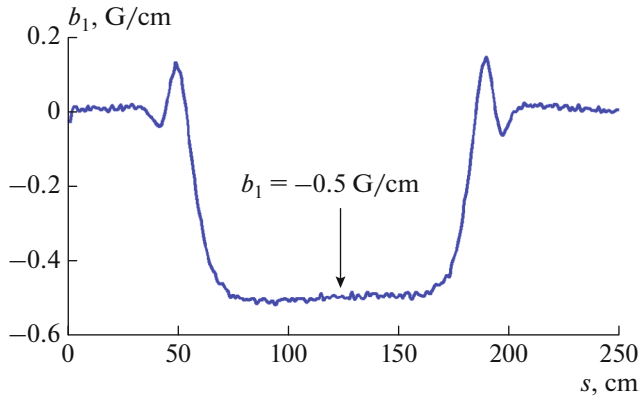

Fig. 13. Radial gradient of the bending magnetic field. The value of the bending field $B_v = 110$ G, bending radius 100 cm.

need to preserve the shape of the beam during its transportation in a longitudinal magnetic field. Otherwise, the beam will be stretched in the transverse direction, acquiring an elliptical shape, which may have a negative impact on its recuperation and on the efficiency of the cooling process.

CONCLUSIONS

When implementing the electron cooling system of the NICA accelerator complex, a detailed study of the quality of the magnetic field in bending magnets was carried out. The measurements were made both with the help of a specialized three-coordinate magnetic field sensor, which allows measuring three field components at one point, and with the help of a set of magnetic field sensors in the vicinity of the central line. It is shown that the measurement results are in good

agreement with the calculation results. For the bending field, the measured field index of 0.45 was in good agreement with the design value of 0.5.

REFERENCES

1. V. B. Reva, et al., "COSY 2 MeV cooler: design, diagnostic and commissioning," in *Proceedings of IPAC (2014) Conference, Dresden, Germany*, pp. 777–779.
2. V. B. Reva, M. I. Bryzgunov, A. V. Bubley, A. D. Goncharov, N. S. Kremnev, V. M. Panasyuk, V. V. Parkhomchuk, V. A. Polukhin, and A. A. Putmakov, "High voltage cooler NICA status and ideas," in *Proceedings of COOL2017 Conference, Bonn, Germany, 2017*, paper TUM21.
3. V. N. Bocharov, A. V. Bublei, S. G. Konstantinov, V. M. Panasyuk, and V. V. Parkhomchuk, "Precision measurements and compensation for the transverse components of the solenoids' magnetic field," Instrum. Exp. Tech. **48**, 772–779 (2005).
4. V. N. Bocharov, M. I. Bryzgunov, A. V. Bubley, V. G. Cheskidov, M. G. Fedotov, V. V. Parkhomchuk, and V. B. Reva, "System for measurement of magnetic field line straightness in solenoid of electron cooler for COSY," in *Proceedings of COOL'11 Conference, Alushta, Ukraine*, pp. 107–110.
5. A. Batrakov, S. Zverev, I. Ilyin, V. Kozak, E. Kuper, V. Mamkin, V. Ovchar, G. Fatkin, V. Tsukanov, P. Vobly, and A. Volkov, "The new VME-based system for magnetic measurements with hall sensors," Preprint Budker Inst. Nucl. Phys. (INP, Novosibirsk, 2007).
6. MV2: Reference sheet/MetroLab. [Web document]. https://www.metrolab.com/wp-content/uploads/2020/06/MagVector-MV2-Datasheet-v2.5.pdf.
7. G. V. Karpov, A. S. Medvedko, and E. I. Shubin, "Precise magnetometers on base of pulsed NMR techniques," in *Proceedings of RuPAC2006 Conference, Novosibirsk, Russia, 2006*, pp. 58–60.